Journal of South American Earth Sciences 79 (2017) 239–253

Contents lists available at ScienceDirect

Journal of South American Earth Sciences

journal homepage: www.elsevier.com/locate/jsames

Famatinian inner arc: Petrographical observations and geochronological constraints on pegmatites and leucogranites of the Comechingones pegmatitic field (Sierras de Córdoba, Argentina)

Manuel Demartis [a, *], Stefan Jung [b], Jasper Berndt [c], Eugenio Aragón [d], Ana María Sato [d], Stefania Radice [a], María Natalia Maffini [a], Jorge Enrique Coniglio [e], Lucio Pedro Pinotti [a], Fernando Javier D'Eramo [a], Leonardo Alfredo Agulleiro Insúa [e]

[a] CONICET – Departamento de Geología, Universidad Nacional de Río Cuarto, Ruta Nacional N° 36 Km 601, CP X5804BYA Río Cuarto, Argentina
[b] Universität Hamburg, Fachbereich Geowissenschaften, Mineralogisch-Petrographisches Institut, Grindelallee 48, 20146 Hamburg, Germany
[c] Institut für Mineralogie, Westfälische Wilhelms-Universität Münster, Corrensstr. 24, D-48149 Münster, Germany
[d] Centro de Investigaciones Geológicas (CONICET - Universidad Nacional de La Plata), Diagonal 113 N° 275, CP B1904DPK La Plata, Argentina
[e] Departamento de Geología, Universidad Nacional de Río Cuarto, Ruta Nacional N° 36 Km 601, CP X5804BYA Río Cuarto, Argentina

ARTICLE INFO

Article history:
Received 2 March 2017
Received in revised form
2 August 2017
Accepted 15 August 2017
Available online 17 August 2017

Keywords:
Granitic pegmatite
Leucogranite
U-Pb LA-ICP MS zircon geochronology
Famatinian magmatism
Sierras Pampeanas

ABSTRACT

The Comechingones pegmatitic field comprises granitic pegmatites and leucogranites hosted by mylonitic rocks from the Guacha Corral shear zone. Pegmatites consist of variably sized, internally zoned bodies, with late replacement units. Leucogranites are fine-grained rocks that form small bodies with tabular-to lens-like shapes. Field relationships and petrographic observations suggest a synkinematic emplacement of both rock types with respect to the main deformational event of this shear zone. U-Pb LA-ICP-MS analyses on zircon crystals indicate crystallization ages of 473.8 ± 3.9 and 474.8 ± 12.2 Ma for the granitic pegmatites and leucogranites, respectively, suggesting that they originated coevally at around 474 Ma. This age provides a first-order time constraint on the deformation of the Guacha Corral shear zone. Using ages and pressure estimations, along with an average pressure gradient of 1GPa/35 km for the continental crust, an exhumation rate of approximately 0.1 mm/a and 10.5 km of total amount of exhumation were calculated for the time span between the early Ordovician and the late Devonian in this part of the Sierras Pampeanas. The inherited ages obtained in zircon crystals from the leucogranites display a distribution pattern that strongly resembles those of the metasedimentary rocks of the Pampean metamorphic belt, suggesting that equivalents of these rocks should have been involved in the melting processes that originated the leucogranites.

1. Introduction

The western margin of Gondwana experienced a complex geodynamic evolution between the late Proterozoic and the late Paleozoic. The Sierras Pampeanas geological province, northwestern Argentina, is constituted by basement blocks that record part of this history, whose most important orogenies were the Pampean and Famatinian. The Pampean orogeny took place between the late Proterozoic to the middle Cambrian. Its best representative rocks are metasediments and arc-related igneous rocks well exposed in the Eastern Sierras Pampeanas and the Puncoviscana formation (Eastern Cordillera and Puna geological provinces).

The Famatinian orogeny spanned from the late Cambrian to the Ordovician, although some authors include Silurian to Carboniferous deformational events as late to post-orogenic stages of this orogeny (Sato et al., 2003). The Famatinian arc and other magmatic rocks of this age are well represented and exposed at the central and western portions of the Sierras Pampeanas geological province, including several mountain ranges such as Sierra de Velasco, Famatina system, Sierra de Chepes, Sierra de San Luis (Baldo et al., 2003; Dahlquist et al., 2008; Morosini and Ortiz Suárez, 2010; Pankhurst et al., 2000; Steenken et al., 2006), and Sierra de Valle Fértil (Otamendi et al., 2009; Ducea et al., 2010; Cristofolini et al.,

* Corresponding author.
E-mail address: mdemartis@exa.unrc.edu.ar (M. Demartis).

http://dx.doi.org/10.1016/j.jsames.2017.08.010
0895-9811/

2014). By contrast, the occurrence of igneous rocks of Famatinian age in the Sierras de Córdoba is much less abundant. They are restricted to small tonalitic and trondhjemitic plutons (Güiraldes, La Fronda, San Agustín, Calmayo and El Hongo plutons), and a few other small igneous bodies of granitic, granodioritic and tonalitic compositions as well (Rapela et al., 1998; D'Eramo et al., 2013, 2014). According to D'Eramo et al. (2014), the Famatinian magmatism in the Sierras de Córdoba has a complex history with compositionally different igneous rocks that emplaced towards the foreland of the main arc. A chemical and chronological zoning is characteristic. Sodium-rich plutons (mostly trondhjemites and tonalites) emplaced in the easternmost side of the Sierras de Córdoba, a few million years earlier (middle to late Cambrian) than the main arc development. These plutons are interpreted as an inner cordilleran belt separated from the main Famatinian arc by back-arc basins (Rapela et al., 1998). Meanwhile, granitic and granodioritic intrusives occur in the western part of the Sierras de Córdoba with dominant early Ordovician ages, coeval with Famatinian ages obtained in other parts of Eastern Sierras Pampeanas (Famatina system, Sierras de San Luis, Valle Fértil, Chepes and Ulapes, among others). Geochronological constraints of these granitic and granodioritic rocks of the Sierras de Córdoba are still poorly addressed (Pankhurst et al., 2000; Steenken et al., 2010; Sfragulla, 2013). The scarcity of geochronological data hampers a good understanding of these events.

In this contribution we present new petrographical and geochronological data of pegmatites and leucogranites from the Comechingones pegmatitic field, cropping out at the west of the Sierras de Córdoba a few hundred kilometers eastwards from the main Famatinian arc magmatic rocks. The pegmatites and leucogranites were emplaced synkinematically with the main deformational event that took place in the Sierras de Córdoba during the earlier times of the Famatinian orogeny. By complementing different sources of information, we will discuss 1) the crystallization age of the studied pegmatites and leucogranites, 2) the timing and exhumation rate of the Guacha Corral shear zone, and 3) the protoliths that probably melted to generate the pegmatites and leucogranites of the study area. The geochronological information here reported constitutes one of the few age constraints on granitic pegmatites from the Sierras Pampeanas carried out by *in situ* techniques (LA-ICP-MS) on zircon crystals.

2. Geological setting

The Comechingones pegmatitic field (CPF) is located in the Sierras de Córdoba, Argentina (Fig. 1). The Sierras de Córdoba constitute the southern end of the Geological Province of Sierras Pampeanas, and comprise a series of mountain ranges trending approximately North-South, consisting of pre-Andean basement blocks that were finally uplifted to the current position by reverse faults during the Andean orogeny. They are mostly composed of metasedimentary and igneous rocks of Precambrian to Devonian age, locally covered by sedimentary and volcanosedimentary sequences mainly of Cretaceous ages.

Two major pre-Carboniferous orogenies have been recognized in the Sierras Pampeanas (Rapela et al., 1998; Ramos, 1999 and references therein): the Pampean and the Famatinian orogenies. Sims et al. (1998) and Stuart-Smith et al. (1999) defined a new cycle, called “Achalian”, to include tectonic and magmatic events that took place during predominantly Devonian times. During the Pampean orogeny, at least two tectono-thermal events took place in the Sierras de Córdoba. The first one was a regional medium-grade metamorphism that developed paragneisses and schists, among other rocks. The ongoing increase in the P-T conditions led to a second event in which deformation and upper amphibolite to granulite facies metamorphism with migmatization and peraluminous magmatism occurred, reaching peak metamorphic conditions of ~7.5 kb and >800 °C (Rapela et al., 1998; Otamendi et al., 2004; Fagiano, 2007; Radice et al., 2015). Paragneisses, metatexites, diatexites and peraluminous granites constitute the most representative rock types. The metasedimentary rocks of the Sierras de Córdoba are regarded as higher grade equivalents of the metaturbidites of the Puncoviscana formation (Ježek et al., 1985; Toselli, 1990; Rapela et al., 1998; Schwartz and Gromet, 2004).

The onset of the Famatinian orogeny in the Sierras Pampeanas is marked by magmatic, metamorphic and deformational events that occurred between late Cambrian to middle Ordovician. In the Sierras de Córdoba, the Famatinian igneous rocks are restricted to small bodies of different compositions with subordinated areal representation. Shearing events ranging in age from early Ordovician to late Devonian (ca. 480 to ca. 365 Ma; Sims et al., 1998; Whitmeyer and Simpson, 2003; Steenken et al., 2010), reworked previous metamorphic fabrics developed during the Pampean orogeny, especially along several major shear zones of the Sierras de Córdoba. Among them, the Guacha Corral shear zone (GCSZ; Fig. 1b) is the largest and most complex of the Sierras de Córdoba (Martino, 2003; Whitmeyer and Simpson, 2003; Otamendi et al., 2004; Fagiano, 2007; Radice et al., 2015). It is a ~120 km long by 20 km wide shear belt that crops out in the central part of the Sierras de Córdoba, with a North–South trend, eastward dip and moderate dipping angle. The main deformational stage of the GCSZ, called M3a-D3a (according to Fagiano et al., 2004; Otamendi et al., 2004; Fagiano, 2007; Cristofolini et al., 2008; Radice et al., 2015), occurred under ductile, medium-to high-grade amphibolite facies conditions, represented by biotite- and sillimanite-bearing mylonitic rocks (Martino et al., 1995; Martino, 2003; Whitmeyer and Simpson, 2003; Fagiano and Martino, 2004; Fagiano et al., 2004; Otamendi et al., 2004; Fagiano, 2007; Cristofolini et al., 2008; Steenken et al., 2010; Demartis et al., 2011; Radice et al., 2012, 2015). Further deformation and greenschist facies metamorphism took place under ductile-brittle conditions leading to a retrogression of the former paragenesis and the local generation of chlorite- and sericite-bearing phyllonites. Kink folding is frequently developed in the Chl + Ser phyllonites. This retrograde metamorphic event was called M3b-D3b and was developed along thin belts interspersed throughout the shear zone (Martino, 2003; Fagiano et al., 2004; Otamendi et al., 2004; Fagiano, 2007; Cristofolini et al., 2008; Radice et al., 2015). In the eastern Sierra de Comechingones, Córdoba province, Radice et al. (2015) give P-T paths for the metamorphic and deformational evolution of the metasedimentary rocks, involving processes occurred during both Pampean and Famatinian orogenies.

Late to post-Famatinian granites, such as the Cerro Áspero and Achala batholiths (Fig. 1b), intruded the GCSZ in the Sierras de Córdoba. They produce thermal aureoles and display discordant polygonal contacts with the mylonitic country rocks, evidencing post-tectonic intrusion with respect to this mylonitic event (Pinotti et al., 2002, 2006). They are thought to have been emplaced after the collision of the Precordillera terrane and during the waning of the Famatinian tectonic activity or during the Achalian orogeny (Rapela et al., 1998; Sims et al., 1998; Stuart-Smith et al., 1999; Pinotti et al., 2014; Lira and Sfragulla, 2014; among others).

Previous geochronological studies performed in detrital zircon, metamorphic overgrowth and igneous crystallization ages on metasedimentary and igneous rocks of Pampean and Famatinian age in the Sierras de Córdoba and other parts of the Sierras Pampeanas are summarized in Table 1.

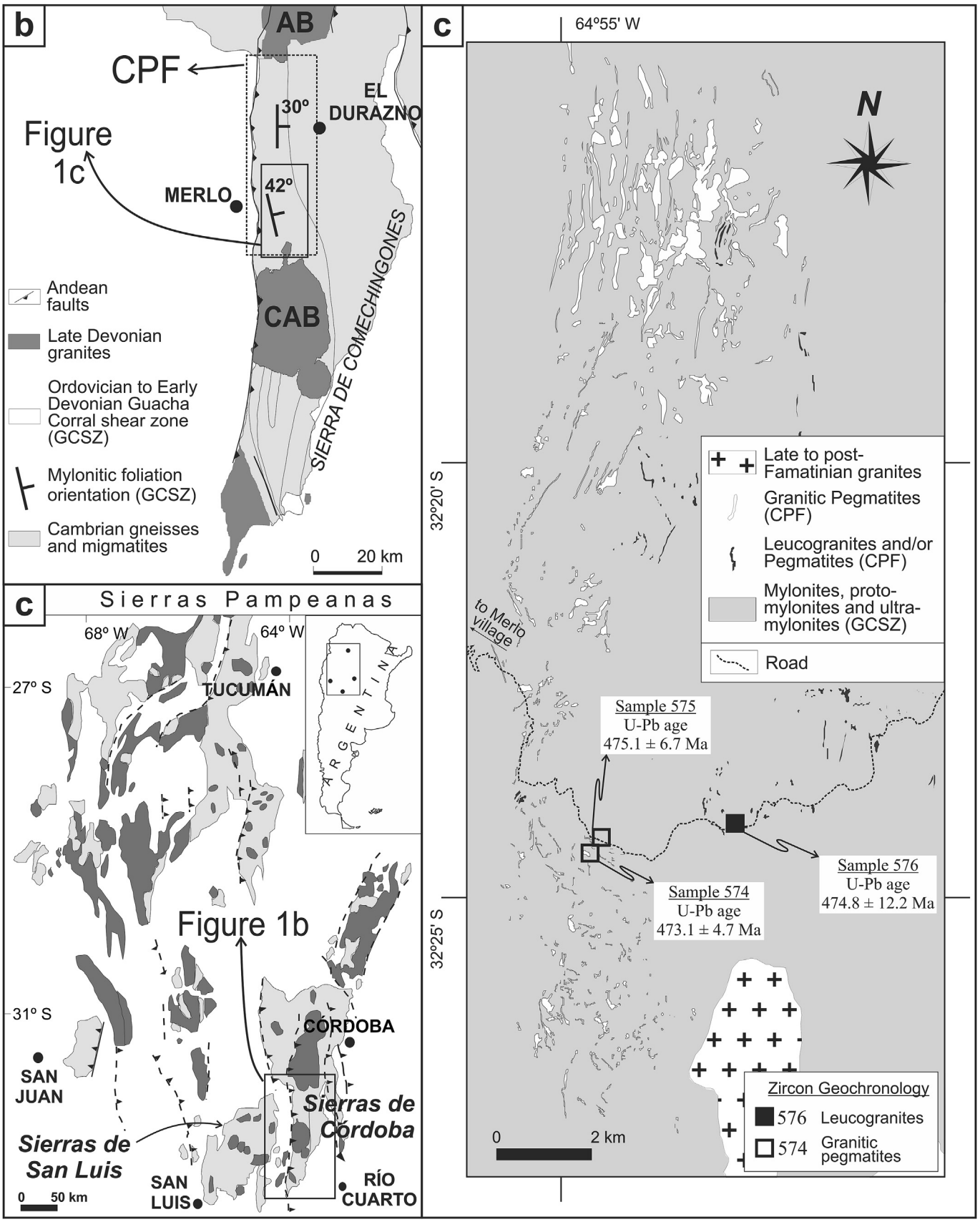

Fig. 1. **a)** Geological sketch of the Sierras Pampeanas, Argentina, showing the position of the Sierras de Córdoba and Sierra de Comechingones. **b)** Simplified geological map of the Sierra de Comechingones showing the extent of the Guacha Corral shear zone. The heavily lined rectangle indicates the extension of Fig. 1c, and the dashed rectangle corresponds to the Comechingones pegmatitic field. CAB: Cerro Áspero Batholith; AB: Achala Batholith. **c)** Simplified geologic map of the granitic pegmatites and leucogranites from the Comechingones pegmatitic field. Crystallization ages obtained for each sample are also shown (see Discussion in the text).

Table 1
Summary of previous geochronological data on rocks from the Pampean and Famatinian orogenies.

Rock, unit or locality and province	Ages or age ranges (Ma) and [number of analyses]	Source type, analytical technique and/or analysis location	Reference
Detrital zircon ages from metamorphic rocks (Pampean belt)			
Grt–Btgneiss (Sierras Chicas) Córdoba province	~700; ~1050; ~1250; 1860; 2550; 2650 [90]	Peaks in probability density plots SHRIMP in zircon	Escayola et al. (2007)
Bt gneiss (San Carlos migmatitic massif) Córdoba province	620; 710; 780; ~1060; 1730; 2530 [65]		
Phyllite (Los Túneles locality) Córdoba province	580; 640; ~1030; 1670; 1890; 2690 [63]		
Grt gneiss (Quilpo formation) Córdoba province	650; 940; 1090; 1440; 1950; 2540 [23]	Peaks in probability density plots SHRIMP in zircon cores	Sims et al. (1998)
Bt–Ms gneiss (Pichanas complex) Córdoba province	610; 660; ~980; 1070; 1620; 2540 [20]		
Peliticgneiss (near Villa de Soto village) Córdoba province	600; 660; 720; ~1020; ~1900 [54]	Peaks in probability density plots Direct evaporation in zircon	Schwartz and Gromet (2004)
Grtmigmatite (La Calera group) Córdoba province	600–650; 800–1000; ~1400	Clusters of $^{207}Pb/^{206}Pb$ ages SHRIMP in zircon	Rapela et al. (1998)
Orthogneiss (Monte Guazú complex) Córdoba province	580; 630; 670; 730; 810; 920–1120; 1830; 1940 [25]	Peaks and age ranges in probability density plots SHRIMP in zircon	Drobe et al. (2011)
Banded schist (Ancasti formation) Catamarca province	570–680; ~830; 960 –1020; 1850–2040 [73]	Peaks and age ranges in probability density plots SHRIMP in zircon	Rapela et al. (2007)
Quartzitegneiss (Sierra Norte) Córdoba province	560; ~600; ~970; 1130; 1530; 1850; 1950; 2670 [59]	Peaks in probability density plots SHRIMP in zircon	Iannizzotto et al. (2013)
Ages of metamorphic overgrowths during Pampean orogeny			
Diatexitic migmatite (Cañada del Sauce) Córdoba province	577 ± 11 [7]	Concordia age SHRIMP in zircon	Siegesmund et al. (2010)
Grt–Bt gneiss (Las Palmas locality) Córdoba province	543.4 ± 3.6 [7]		
Stromatite (Tala Cruz) Córdoba province	553.5 ± 3.2 [5]		
Grt–Crd granulites (Santa Rosa locality) Córdoba province	536 ± 11 [4]	Concordia age SHRIMP in zircon	
	514 ± 5.1 [6]; 545.4 ± 6.9 [3]	Concordia age SHRIMP in monazite	
Diatexitic migmatite (San Carlos massif) Córdoba province	496.2 ± 9.1 [2]	Concordia age SHRIMP in zircon	
Bt–Ms gneiss (Pichanas complex) Córdoba province	531 ± 10; 561 ± 10 [14]	Peaks in probability density plots SHRIMP in zircon rims	Sims et al. (1998)
Grt gneiss (Quilpo formation) Córdoba province	529 ± 10; 585 ± 16 [16]		
Bt gneiss (San Carlos migmatitic massif) Córdoba province	525 ± 52	Metamorphic rims SHRIMP in zircon	Escayola et al. (2007)
Grt migmatite (La Calera group) Córdoba province	522 ± 8 [17]	Weighted mean $^{206}Pb/^{238}U$ ages SHRIMP in monazite	Rapela et al. (1998)
Crystallization ages of igneous rocks from the Famatinian arc			
Trondhjemite (Calmayo& El Hongoplutons; Sierras de Córdoba) Córdoba province	501 ± 4 [3]; 512 ± 3 [4]	Weighted mean $^{206}Pb/^{238}U$ ages Conventional analyses in zircon	D'Eramo et al. (2013)
Trondhjemite (Güiraldes pluton; Sierras de Córdoba) Córdoba province	499 ± 6 [18]	Weighted mean $^{206}Pb/^{238}U$ age SHRIMP in zircon	Rapela et al. (1998)
Granitic pegmatites (Sierra de Comechingones) Córdoba province	486 ± 7; 487 ± 10	K-Ar age in muscovite	Steenken et al. (2010)
Granodiorite, granite, gabbro (Sierras de los Llanos, Malanzán & Chepes) La Rioja province	479–496	Different sources	Pankhurst et al. (1998)
Tonalite (Las Verbenas pluton, Sierra de San Luis) San Luis province	478 ± 4 [18]	Concordia age SHRIMP in zircon	Steenken et al. (2006)
Porphyritic Bt granite (La Escalerilla pluton, Sierra de San Luis) San Luis province	477 ± 12 [8]	Concordia age LA-MC-ICP-MS in zircon	Morosini et al. (2017)
Tur – Bt granite (La Yeya Norte pluton, western Sierras de Córdoba) Córdoba province	471 + 9/-32	Zircon U-Pb age	Sfragulla (2013)
Diorite, gabbro, granodiorite, granite, tonalite, migmatite (Sierra de Valle Fértil) San Juan province	469–492 [272]	Weighted mean $^{206}Pb/^{238}U$ ages LA-MC-ICP-MS in zircon	Ducea et al. (2010)
Granites, granodiorites, and gabbros of I- and S-typeaffinities (Sierras de Córdoba, Chepes, Los Llanos, Valle Fértil, Famatina, Velasco, Mazán, Capillitas) Córdoba, La Rioja, Catamarca and San Juan provinces	468–484 [188]	Weighted mean $^{206}Pb/^{238}U$ ages SHRIMP in zircon	Pankhurst et al. (2000)
Porphyritic rhyolite (near Chaschuil, Famatina system) Catamarca province	468 ± 3 [15]	Weighted mean $^{206}Pb/^{238}U$ ages SHRIMP in zircon	Baldo et al. (2003); Fanning et al. (2004)
Tonalite, monzogranite, rhyolite (Sierra de Famatina) La Rioja province	463 ± 4 [8]; 477 ± 4 [8]; 481 ± 4 [8]	Weighted mean $^{206}Pb/^{238}U$ ages SHRIMP in zircon	Dahlquist et al. (2008)

3. Field relationships and petrography of the CPF

The CPF groups pegmatites of granitic composition (granitic pegmatites) and aplitic leucogranites that crop out in the northern Sierra de Comechingones (Fig. 1b), hosted by mylonitic rocks of the GCSZ (Angelelli, 1950; Rinaldi, 1968, 1969; Methol, 1971; Hub, 1994, 1995; Demartis, 2010; Demartis et al., 2011). Quartz-rich dikes with pegmatitic textures also occur in the eastern part of the CPF (Demartis, 2010; Morteani et al., 2012, 2016). The granitic pegmatites belong to the LCT geochemical signature, and they were classified as muscovite- and rare element-class, beryl-columbite-phosphate subtype pegmatites (Galliski, 1994), and recently reclassified as belonging to the muscovite – rare-element class of Černý and Ercit (2005) (Demartis, 2010).

Pegmatites and leucogranites of the CPF are hosted by strongly deformed mica-rich schists with conspicuous mylonitic textures. Protoliths of these mylonites are mostly stromatic metatexites and, to a lesser extent, diatexites and gneisses generated during the Pampean orogeny. From non-deformed migmatites to mylonites and ultramylonites several textural, structural and mineralogical changes can be observed. Quartz-feldspar leucosomes from the stromatites are progressively stretched and boudinaged, becoming completely dismembered and constituting porphyroclasts with further deformation. Porphyroclasts of quartz-feldspar aggregates, garnet and cordierite, with ubiquitous pressure shadows, are wrapped by a mylonitic foliation, composed of recrystallized quartz, biotite and sillimanite that formerly constituted the melanosomes of the stromatites. Biotite experienced a drastic grain size reduction and prismatic sillimanite was completely fibrolitized during deformation. The parallel arrangement of the recrystallized biotite and fibrolite, along with the orientation of quartz ribbons, defines an anastomosing pattern of the mylonitic foliation. Other textures and structures, such as fish-shaped micas and S/C structures, are very frequent. Late retrograde deformation partially or totally overprints the mylonites into phylonites with a chlorite + muscovite matrix. These changes reveal an east-to-west progressive increase in the intensity of deformation at the Merlo village latitude (Fig. 1c), also observed by other authors (Simpson et al., 2003; Whitmeyer and Simpson, 2003; Fagiano et al., 2004; Otamendi et al., 2004; Fagiano, 2007; Cristofolini et al., 2008; Steenken et al., 2010; Demartis et al., 2011; Radice, 2015).

The granitic pegmatites crop out mostly in the western part of the studied area (Fig. 1c) where host mylonites are most intensely deformed. Granitic pegmatites are found as composite pegmatitic bodies (Demartis et al., 2011) with variable sizes. They are granitic in composition, with accessory minerals including garnet, Fe-Mn phosphates, uraninite, beryl and columbite-group minerals. They commonly show a well-zoned internal structure consisting of 3 or 4 internal zones (wall, intermediate and core zones). Late-stage replacement units with extreme enrichment in some elements (Li, Cs, F, Ta, Hf, etc) occur in a few pegmatites (Demartis et al., 2014). Mean planar orientation of the pegmatite bodies generally strikes parallel with the pervasive foliation of the mylonitic host rocks. An internal foliation defined by fractured and flattened porphyroclasts of coarse-grained microcline, stretched quartz and preferentially oriented muscovite flakes, are commonly observed in granitic pegmatites (Fig. 2a). Textures and microstructures, such as wedge-shaped intracrystalline fractures filled by residual melt (Fig. 2b), mechanical twins in feldspars, chessboard patterns in quartz, flame-shaped perthites in microcline (Fig. 2c), and undulose extinction and deformation lamellae in quartz, described in all internal zones of granitic pegmatites, point to a continuous deformation from submagmatic to subsolidus conditions, thus suggesting syn-deformational emplacement (Demartis et al., 2011). Leucogranites are typically light colored and have fine-grained (aplitic) textures, with grain size generally lower than 1 mm. They consist of alkali feldspar, quartz and plagioclase, with muscovite, biotite, garnet, apatite, zircon and monazite as accessory phases. According to the IUGS classification, they plot in the boundary between granodiorite and monzogranite. Leucogranites mostly occur in the eastern part of the study area (Fig. 1c), although they can also be found in the western part of the studied area as peripheral units within the granitic pegmatites and individual bodies. They commonly show tabular and lens shapes, generally extending less than 200 m long and a few decimeters wide. Leucogranites frequently crop out conformably and harmonically with respect to the mylonitic foliation of the country rocks (Fig. 2d), although some discordant examples have been also described. The strong preferred orientation of muscovite, biotite and quartz ribbons defines a conspicuous S/C structure observed at both mesoscale (Fig. 2e) and microscale (Fig. 2f). Orientations of the C planes are usually parallel to the host mylonitic foliation. Microfractures filled with residual melt (Bouchez et al., 1992) in plagioclase crystals (Fig. 2g), chessboard extinction patterns in quartz grains (Fig. 2h), oriented fish shapes of muscovite and biotite, and microscale S/C structures also suggest a continuous deformation from submagmatic to subsolidus conditions in the leucogranites. Kinematic analysis at the mesoscale and microscale yielded the same sense of shearing as that obtained in the host mylonitic rocks for the ductile D3a-M3a event. All of these evidences strongly suggest that the leucogranites were synkinematically emplaced with respect to this event, with P-T conditions probably similar to those of the granitic pegmatites.

4. U-Pb zircon geochronology

4.1. Sampling and analytical methods

Granitic pegmatites (sample 574 and 575) and leucogranites (sample 576) from the CPF were analyzed for geochronological purposes. Sample locations and resultant ages are shown in Fig. 1d, and geochronological data are presented in Table 2.

Zircon was separated from the hand specimen by standard heavy mineral separation techniques. The rocks were first crushed, followed by magnetic separation using hand magnet separator to exclude the magnetic minerals. The separate was washed, cleaned and dried to exclude very fine-grained material. Then it was subjected to heavy mineral separation using bromoform liquid. Handpicking extraction of the individual zircon grains was performed under binocular microscope. Selected grains were mounted on epoxy resin discs and polished. Before analysis, cathodoluminescence (CL) and backscattered electron images were performed on the selected zircon crystals in order to study their internal structure and compositional variations. Points were selected on several zircon grains to include all texturally distinct domains in CL images. U-Pb isotopic analyses were carried out by using a ThermoFinnigan Element2 sector field ICP-MS coupled to a New Wave UP193HE ArF Excimer laser system at the Institute for Mineralogie, Westfälische Wilhelms-Universität, Münster, Germany. The analytical details for the measurement of U and Pb isotopes using the LA-ICP-MS are further elaborated by Kooijman et al. (2012).

4.2. Granitic pegmatites

Two granitic pegmatites were analyzed for geochronological purposes. Zircons in both samples (sample 574, 32°24′29.27″S and 64°54′37.11″W; and sample 575, 32°24′18.58″S and 64°54′27.63″W) are large (generally > 150 μm, as long as 500 μm) euhedral, short and long prismatic crystals, with axial ratios commonly between 1:2.5 and 1:5. The zircon crystals from both pegmatite samples (Fig. 3) have patchy textures, and compositional zoning is almost absent in CL images. They are frequently highly metamict, hindering reliable analysis.

Over one hundred spot analyses were carried out in both 574 and 575 samples, but only a few of them were useful. Most of the analyses exhibited high errors, low concordance percentage and/or anomalously high common Pb contents, hence they were discarded from the further processing. Uranium contents in these zircons range between 666 and 14809 ppm. Fifteen spot analyses from

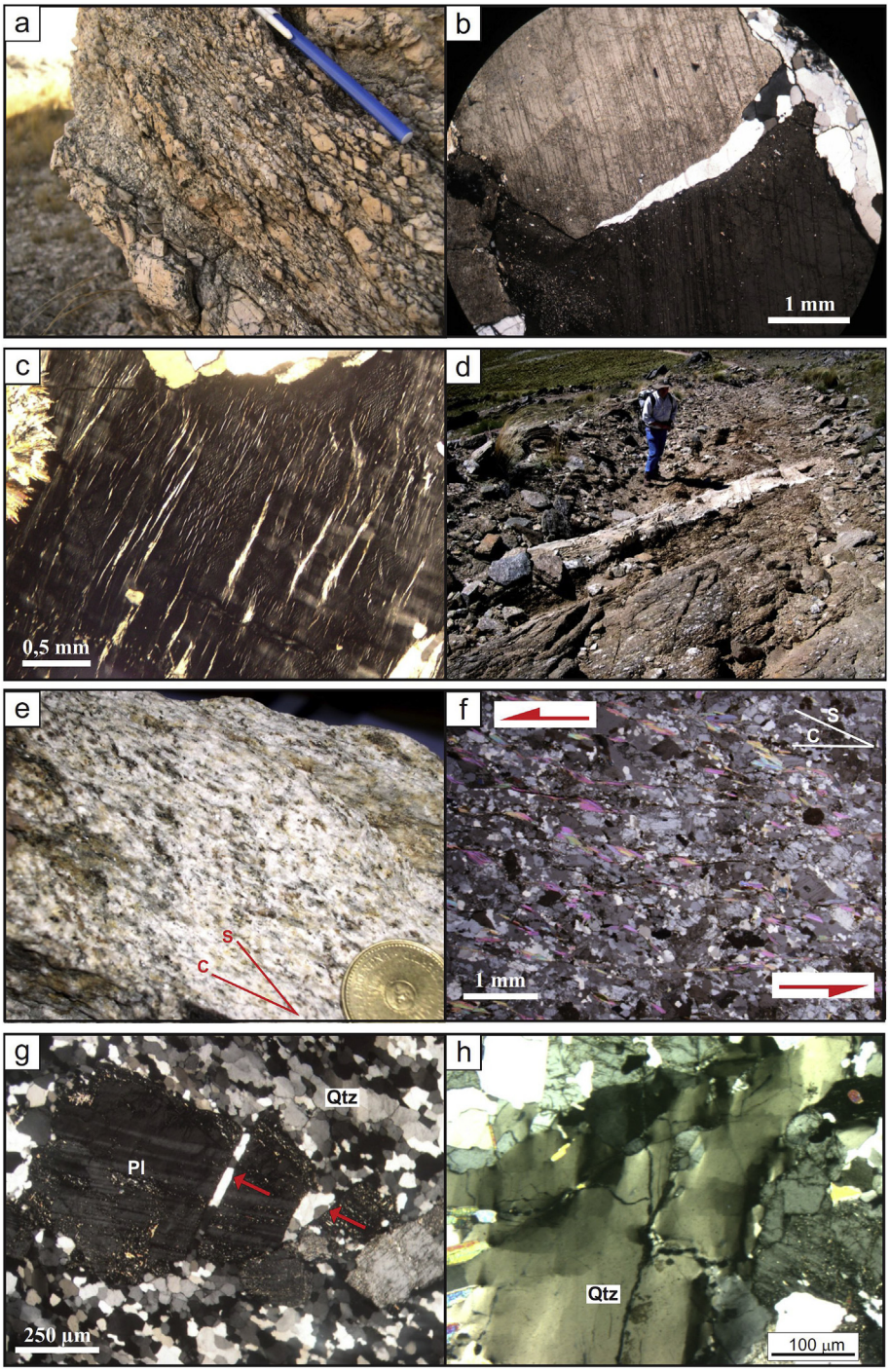

Fig. 2. a) Mylonitic foliation developed in the intermediate zone of a granitic pegmatite, with stretched and reoriented microclines, quartz ribbons, and oriented micas (Demartis et al., 2011). **b)** Wedge-shaped intracrystalline fracture affecting microcline from the intermediate zone of a granitic pegmatitic, infilled with a residual melt, suggesting deformation at submagmatic conditions (Bouchez et al., 1992). Crossed polarizers, XZ-section (Demartis et al., 2011). **c)** Albite flame perthites in large microcline grain from the intermediate zone of a granitic pegmatite. Crossed polarizers (Demartis et al., 2011). **d)** Tabular-shaped body of leucogranite conformable with the mylonitic foliation of the host rocks. The dike is 6 m long and 0.6 m thick. **e)** Hand specimen of leucogranite showing preferred orientation of quartz, feldspars and micas defining S/C structures. **f)** Photomicrograph showing an S/C fabric in leucogranite, with fish-shaped muscovite and quartz ribbons defining the main S and C planes. **g)** Plagioclase crystals in leucogranite with microfractures (red arrows) infilled by residual melt composed of quartz grains (Bouchez et al., 1992). **h)** Chessboard microstructures in quartz crystals from leucogranite conditions. The above mentioned information, along with P-T crystallization conditions (estimated to 500 MPa and 600 °C, respectively; Demartis et al., 2010) and kinematic analysis (Demartis et al., 2011), demonstrates that the granitic pegmatites were emplaced synkinematically with respect to the main ductile event of the GCSZ, with an almost complete reverse sense of shear. (For interpretation of the references to colour in this figure legend, the reader is referred to the web version of this article.)

sample 574 and six from sample 575 remained after selection, which yielded reliable data (Table 2).

Eight spot analyses with discordances between 90 and 110% (11-1, 15-1, 16-1, 17-1, 21-2, 25-2, 27-1 and 31-1; Table 2) were selected from the sample 574 to calculate a weighted mean concordia age, yielding an age of 473.1 ± 4.7 Ma (2σ; MSWD = 0.035; Fig. 4a). A

Table 2
LA-ICPMS U-Pb zircon results for granitic pegmatites (samples 574 and 575) and leucogranites (sample 576).

# Analysis	Isotopic ratios								Apparent ages (Ma)									
	U (ppm)	$^{206}Pb/^{238}U$	±2σ	$^{207}Pb/^{235}U$	±2σ	$^{207}Pb/^{206}Pb$	±2σ	Error Corr.	$^{206}Pb/^{238}U$	±2σ	±2σ%	$^{207}Pb/^{235}U$	±2σ	±2σ%	$^{207}Pb/^{206}Pb$	±2σ	±2σ%	Conc. (%)
Granitic pegmatite - Sample 574																		
1–1	2999	0.07649	0.00242	0.61736	0.02107	0.05854	0.00075	0.93	475.1	14.5	3.1	488.2	13.2	2.7	550.1	28.0	5.1	86.4
5–1	6035	0.07672	0.00311	0.58481	0.04186	0.05529	0.00326	0.57	476.5	18.6	3.9	467.6	26.8	5.7	424.0	131.9	31.1	112.4
8–2	3893	0.07645	0.00254	0.56000	0.06233	0.05312	0.00564	0.30	474.9	15.2	3.2	451.5	40.6	9.0	334.1	242.5	72.6	142.1
11–1	4829	0.07618	0.00206	0.58928	0.01803	0.05610	0.00081	0.88	473.3	12.3	2.6	470.4	11.5	2.4	456.6	32.0	7.0	103.7
14–2	2041	0.07753	0.00202	0.58904	0.02487	0.05510	0.00183	0.62	481.3	12.1	2.5	470.3	15.9	3.4	416.5	74.3	17.8	115.6
15–1	7409	0.07757	0.00216	0.60760	0.01818	0.05681	0.00063	0.93	481.6	12.9	2.7	482.0	11.5	2.4	484.2	24.5	5.0	99.5
16–1	2111	0.07564	0.00202	0.58960	0.04213	0.05653	0.00375	0.37	470.0	12.1	2.6	470.6	26.9	5.7	473.5	147.0	31.0	99.3
17–1	2338	0.07502	0.00185	0.58267	0.02691	0.05633	0.00220	0.53	466.3	11.1	2.4	466.2	17.3	3.7	465.4	86.6	18.6	100.2
21–2	2096	0.07561	0.00282	0.58959	0.10067	0.05656	0.00942	0.22	469.8	16.9	3.6	470.6	64.4	13.7	474.4	374.9	79.0	99.0
25–1	698	0.07873	0.00323	0.59583	0.05695	0.05488	0.00474	0.43	488.5	19.3	4.0	474.6	36.2	7.6	407.6	194.0	47.6	119.9
25–2	666	0.07962	0.00283	0.61775	0.04664	0.05627	0.00375	0.47	493.8	16.9	3.4	488.4	29.3	6.0	463.3	148.0	32.0	106.6
25–3	1352	0.07607	0.00339	0.61168	0.03383	0.05832	0.00191	0.81	472.6	20.3	4.3	484.6	21.3	4.4	541.7	71.7	13.2	87.2
27–1	4232	0.07582	0.00328	0.59112	0.02649	0.05655	0.00065	0.97	471.1	19.7	4.2	471.6	16.9	3.6	473.9	25.5	5.4	99.4
29–1	6096	0.07241	0.00316	0.57758	0.03272	0.05785	0.00209	0.77	450.6	19.0	4.2	462.9	21.1	4.6	524.2	79.3	15.1	86.0
31–1	2636	0.07461	0.00319	0.57723	0.02770	0.05611	0.00122	0.89	463.9	19.1	4.1	462.7	17.8	3.9	456.8	48.3	10.6	101.5
Granitic pegmatite - Sample 575																		
7–1	7156	0.07724	0.00180	0.62695	0.01708	0.05887	0.00082	0.86	479.6	10.8	2.3	494.2	10.7	2.2	562.2	30.5	5.4	85.3
10–1	6638	0.07698	0.00169	0.59827	0.03706	0.05636	0.00327	0.35	478.1	10.1	2.1	476.1	23.5	4.9	466.8	128.6	27.5	102.4
21–1	14809	0.07572	0.00214	0.61369	0.01896	0.05878	0.00073	0.92	470.5	12.8	2.7	485.9	11.9	2.5	559.1	27.1	4.9	84.2
21–2	11786	0.06234	0.00185	0.49901	0.01643	0.05806	0.00083	0.90	389.8	11.2	2.9	411.0	11.1	2.7	531.9	31.3	5.9	73.3
28–1	3890	0.07607	0.00148	0.60280	0.03047	0.05747	0.00268	0.39	472.6	8.9	1.9	479.0	19.3	4.0	509.8	102.7	20.1	92.7
28–2	12724	0.07720	0.00142	0.61682	0.01301	0.05795	0.00060	0.87	479.4	8.5	1.8	487.9	8.2	1.7	527.9	22.7	4.3	90.8
Leucogranite - Sample 576																		
1–1	239	0.09555	0.00228	0.78133	0.02169	0.05931	0.00085	0.86	588.3	13.4	2.3	586.2	12.4	2.1	578.4	31.0	5.4	101.7
2–1	210	0.24877	0.00665	3.08813	0.09793	0.09003	0.00154	0.84	1432.1	34.3	2.4	1429.7	24.3	1.7	1426.3	32.6	2.3	100.4
3–1	205	0.05908	0.00176	0.43880	0.01743	0.05387	0.00142	0.75	370.0	10.7	2.9	369.4	12.3	3.3	365.5	59.4	16.3	101.2
4–1	213	0.09248	0.00254	0.74612	0.02374	0.05851	0.00094	0.86	570.2	15.0	2.6	566.0	13.8	2.4	549.1	35.0	6.4	103.8
6–1	171	0.14613	0.00413	1.36540	0.04352	0.06777	0.00100	0.89	879.2	23.2	2.6	874.2	18.7	2.1	861.6	30.6	3.5	102.0
7–1	73	0.32904	0.01071	5.04225	0.20215	0.11114	0.00260	0.81	1833.6	52.0	2.8	1826.4	34.0	1.9	1818.3	42.5	2.3	100.8
8–1	556	0.07644	0.00204	0.59405	0.01748	0.05637	0.00069	0.91	474.8	12.2	2.6	473.5	11.1	2.4	467.0	27.1	5.8	101.7
9–1	79	0.08261	0.00232	0.68638	0.03352	0.06026	0.00241	0.57	511.7	13.8	2.7	530.6	20.2	3.8	613.0	86.4	14.1	83.5
10–1	280	0.13866	0.00364	1.27549	0.03579	0.06672	0.00067	0.93	837.0	20.6	2.5	834.8	16.0	1.9	829.0	20.8	2.5	101.0
12–1	185	0.06141	0.00228	0.50528	0.02380	0.05967	0.00173	0.79	384.2	13.9	3.6	415.3	16.1	3.9	591.8	62.8	10.6	64.9
12–2	384	0.08758	0.00239	0.79383	0.02645	0.06574	0.00126	0.82	541.2	14.2	2.6	593.3	15.0	2.5	798.2	40.1	5.0	67.8
13–1	528	0.17186	0.00401	1.73645	0.04595	0.07328	0.00092	0.88	1022.3	22.1	2.2	1022.1	17.1	1.7	1021.8	25.3	2.5	100.1
15–1	801	0.10114	0.00201	0.84924	0.03617	0.06090	0.00230	0.47	621.0	11.7	1.9	624.2	19.9	3.2	635.8	81.2	12.8	97.7
15–2	267	0.08592	0.00185	0.68991	0.03928	0.05824	0.00307	0.38	531.3	11.0	2.1	532.7	23.6	4.4	538.9	115.5	21.4	98.6
16–1	440	0.14168	0.00427	1.33090	0.04783	0.06813	0.00133	0.84	854.2	24.1	2.8	859.3	20.8	2.4	872.5	40.6	4.6	97.9
18–1	229	0.10821	0.00247	0.89970	0.02503	0.06030	0.00096	0.82	662.3	14.4	2.2	651.6	13.4	2.1	614.4	34.2	5.6	107.8
18–2	297	0.07655	0.00199	0.68450	0.02344	0.06485	0.00145	0.76	475.5	11.9	2.5	529.5	14.1	2.7	769.5	47.0	6.1	61.8
20–1	62	0.08017	0.00186	0.61947	0.02109	0.05604	0.00140	0.68	497.1	11.1	2.2	489.5	13.2	2.7	454.0	55.3	12.2	109.5
20–2	28	0.08003	0.00231	0.62640	0.03242	0.05677	0.00244	0.56	496.3	13.8	2.8	493.8	20.2	4.1	482.5	94.9	19.7	102.9
22–1	746	0.45096	0.00867	9.67158	0.34402	0.15555	0.00466	0.54	2399.5	38.5	1.6	2404.0	32.7	1.4	2407.9	50.9	2.1	99.7
22–2	260	0.09538	0.00226	0.77879	0.06430	0.05922	0.00468	0.29	587.3	13.3	2.3	584.8	36.7	6.3	575.1	172.6	30.0	102.1
25–3	250	0.11093	0.00114	0.94142	0.01858	0.06155	0.00104	0.52	678.1	6.6	1.0	673.6	9.7	1.4	658.6	36.2	5.5	103.0
26–2	133	0.11833	0.00260	1.03810	0.03203	0.06363	0.00138	0.71	720.9	15.0	2.1	723.0	16.0	2.2	729.3	45.8	6.3	98.9
28–1	81	0.11489	0.00299	0.97104	0.03883	0.06130	0.00186	0.65	701.1	17.3	2.5	689.0	20.0	2.9	649.8	65.2	10.0	107.9
28–2	71	0.08774	0.00227	0.70540	0.02329	0.05831	0.00120	0.78	542.1	13.4	2.5	542.0	13.9	2.6	541.6	44.9	8.3	100.1
32–1	33	0.16711	0.00504	2.35448	0.12659	0.10219	0.00455	0.5606	996.1	27.8	2.8	1228.9	38.3	3.1	1664.3	82.5	5.0	59.9
32–2	74	0.09375	0.00296	0.76520	0.03213	0.05920	0.00164	0.7517	577.6	17.4	3.0	577.0	18.5	3.2	574.5	60.2	10.5	100.5
32–3	160	0.08442	0.00259	0.73376	0.02852	0.06304	0.00150	0.7891	522.4	15.4	2.9	558.8	16.7	3.0	709.5	50.8	7.2	73.6

(*continued on next page*)

Table 2 (*continued*)

# Analysis	Isotopic ratios								Apparent ages (Ma)							
	U (ppm)	$^{206}Pb/^{238}U$	±2σ	$^{207}Pb/^{235}U$	±2σ	$^{207}Pb/^{206}Pb$	±2σ	Error Corr.	$^{206}Pb/^{238}U$	±2σ	±2σ%	$^{207}Pb/^{235}U$	±2σ	±2σ%	$^{207}Pb/^{206}Pb$	±2σ	±2σ%	Conc. (%)
33–1	304	0.11000	0.00352	0.94207	0.03339	0.06212	0.00095	0.9023	672.7	20.4	3.0	674.0	17.5	2.6	678.2	32.7	4.8	99.2
33–2	283	0.08570	0.00234	0.74038	0.02652	0.06266	0.00145	0.7624	530.0	13.9	2.6	562.6	15.5	2.7	696.8	49.4	7.1	76.1
35–1	177	0.16728	0.00520	1.66374	0.05809	0.07214	0.00114	0.8912	997.1	28.7	2.9	994.8	22.1	2.2	989.8	32.2	3.3	100.7
35–2	454	0.08833	0.00257	0.74513	0.02680	0.06118	0.00130	0.8079	545.6	15.2	2.8	565.4	15.6	2.8	645.7	45.6	7.1	84.5
37–2	336	0.11944	0.00273	1.05332	0.02677	0.06396	0.00071	0.8985	727.3	15.7	2.2	730.5	13.2	1.8	740.4	23.6	3.2	98.2

weighted average on $^{206}Pb/^{238}U$ ages was also calculated using the eight concordant spot analyses of the sample 574, giving a mean age of 473.3 ± 7.3 Ma (2σ; MSWD = 1.5; Fig. 4a). Two of the three analysis with discordances between 90 and 110% from sample 575 (10-1 and 28-1; Table 2) have been selected to calculate a concordia age, yielding a result of 475.1 ± 6.7 Ma (2σ; MSWD = 0.19; Fig. 4b). Spot analysis 28-2 was rejected because of its high U content. Since ages from both samples are strongly equivalent to each other, a new weighted mean concordia age was calculated using analyses of both samples, yielding an age of 473.8 ± 3.9 Ma (2σ; MSWD = 0.037; probability of concordance = 0.85; number of analysis = 10).

No inherited ages were obtained for the pegmatites, *i.e.* there are no ages older than 494 Ma. This observation indicates that the analyzed zircon crystals in these rocks were formed exclusively during pegmatite crystallization.

4.3. Leucogranites

Unlike the pegmatites, most zircon crystals from the leucogranites (sample 576, 32°24′7.84″S and 64°52′40.67″W) are almost entirely inherited. They are relatively small (40–200 μm), with a length average of 120 μm. They are typically euhedral to subhedral. Their length-to-width ratios commonly range between 1 and 2.5. Partially resorbed inherited cores are commonly observed in CL images, and they usually show later overgrowth zones (Fig. 5).

Thirty three spots were analyzed in cores and rims from 23 zircon crystals (Table 2; Fig. 6). Ages obtained in this sample span from Paleoproterozoic to late Devonian, but the great majority ranges between ~2400 and 470 Ma, with a high scattering (Table 2; Figs. 6 and 7). Only two ages younger than 470 Ma were obtained, and they yielded $^{206}Pb/^{238}U$ ages of 384.2 ± 13.9 and 370.0 ± 10.7 Ma, with concordance percentages of ~65 and 102%, respectively. The first one was obtained from a core zone with some inclusions and irregular zoning. The remaining Devonian age was performed on a zircon fragment with fine-scale, wedge-shaped oscillatory zoning and some inclusions (Fig. 5). A $^{206}Pb/^{238}U$ age yielding 474.8 ± 12.2 Ma, with a degree of concordance of 102%, was obtained from an inclusion-free, probably prismatic-shaped crystal fragment with broad parallel zoning (Fig. 5; Table 2).

The rest of the analysis from sample 576 span from Paleoproterozoic to early Ordovician times, with degree of concordances ranging between ~60 and 110%. They were carried out in variably shaped zircon grains (short- and long-prismatic, rounded, irregular, etc.), both in cores and rims. Although somewhat variable, cores commonly show high luminescence and oscillatory zoning, while overgrowth rims are usually low luminescent (Fig. 5). The probability density plot of Fig. 7 was constructed using only concordant ages (degree of concordance between 90 and 110%), where ages younger than 1000 Ma are $^{206}Pb/^{238}U$ data, and ages older than 1000 Ma are $^{207}Pb/^{206}Pb$ data. It shows that most of the inherited ages range between 490 and 1022 Ma, with subordinated early Mesoproterozoic and Paleoproterozoic components (three single analyses yielded $^{207}Pb/^{206}Pb$ ages of 1426.3 ± 32.6, 1818.3 ± 42.5 and 2407.9 ± 50.9 Ma). In the range between 490 and 1022 Ma (Fig. 7 - inset) seven peaks at 496, 533, 587, 678, 723, 843 and 988 Ma are clearly defined Ma are clearly defined.

5. Discussion

5.1. Crystallization ages of pegmatites and leucogranites from the CPF

The geochronological data obtained from granitic pegmatites in this study yielded a concordia age of crystallization of 473.8 ± 3.9 Ma based on analysis from samples 574 and 575. The complete

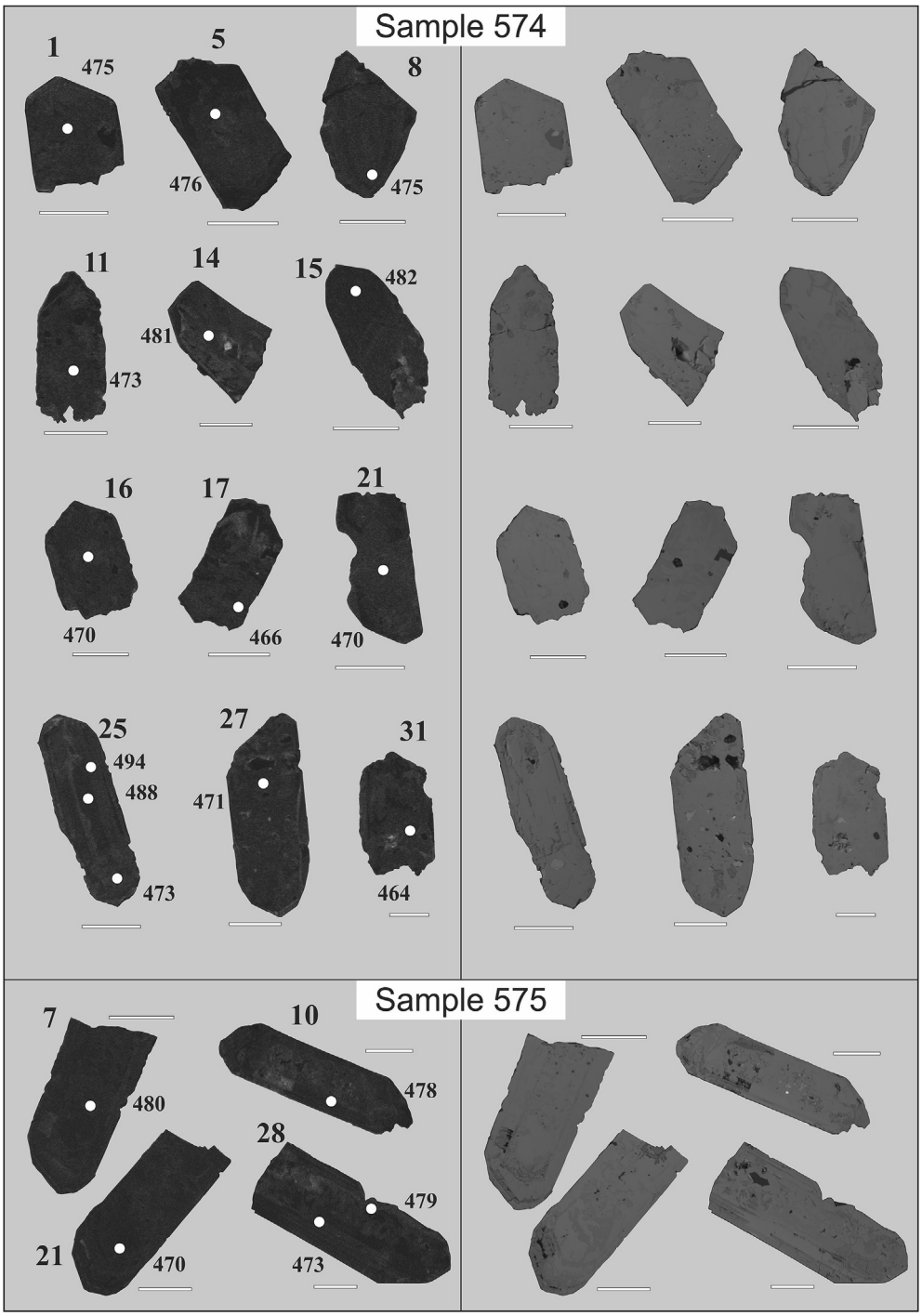

Fig. 3. Cathodoluminiscence (left) and backscattered electron (right) images of analyzed zircon crystals from granitic pegmatite of the CPF (samples 574 and 575). Individual U–Pb spots are shown by white circles and corresponding ages are given as $^{206}Pb/^{238}U$ ages.

absence of ages older than 494 Ma in these samples, along with the crystal shapes and sizes evidencing a primary origin, indicates that these crystals are autocrysts (Miller et al., 2007), *i.e.*, they entirely grew during pegmatite crystallization. We consider here that this age constitutes the best constraint on the timing of crystallization of the granitic pegmatites of the CPF.

In sample 576 (leucogranites), the large scattering of the obtained ages along with the frequent presence of xenocrystic cores suggests that most of the ages obtained in this sample are inherited. Thus, only the youngest ones were selected and evaluated in order to estimate the crystallization age.

The youngest ages obtained in this sample were 384.2 and 370.0 Ma (see above). Analysis 12-1, yielding the age of 384.2 Ma, was discarded since it has 64.9% of concordance. The other age is not deemed to represent the crystallization age of the leucogranites because of the following arguments, mostly based on field relationships and geological context. The late to post-Famatinian Cerro Áspero batholith, which crops out a few kilometers south

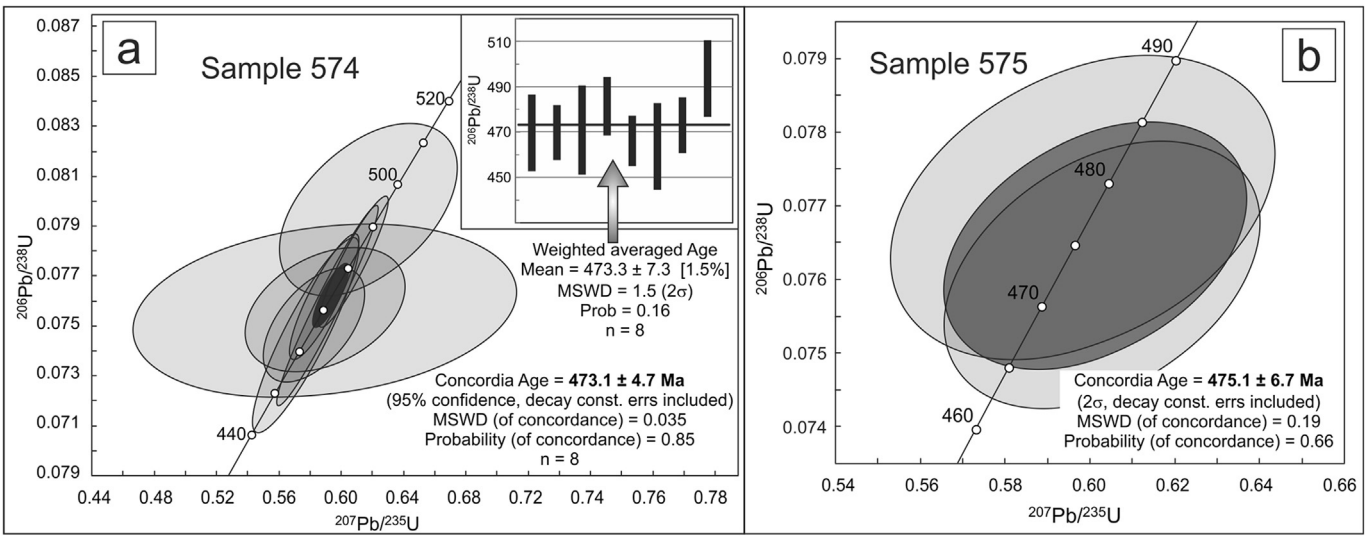

Fig. 4. Concordia diagrams and weighted average plot of granitic pegmatites from **a)** sample 574; **b)** sample 575.

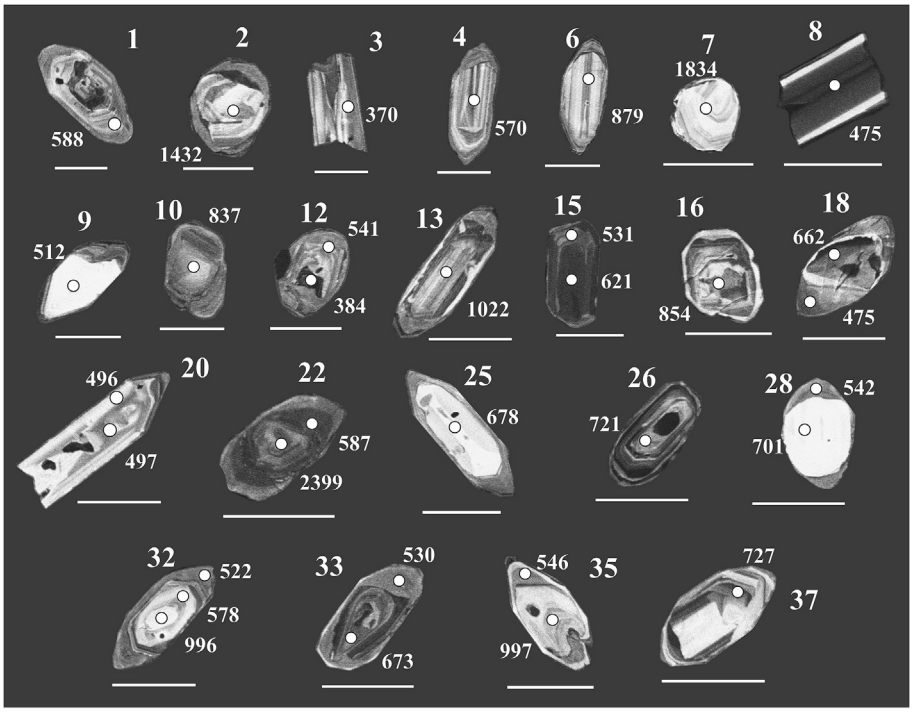

Fig. 5. Cathodoluminiscence images of analyzed zircon crystals from leucogranites of the CPF (sample 576). Individual U–Pb spots are shown by white circles and corresponding ages are given as $^{206}Pb/^{238}U$ ages.

from the leucogranites (Fig. 1), was emplaced at around 200 MPa. According to a Rb-Sr whole rock age, it crystallized at 369 ± 9 Ma (Pinotti et al., 2006, 2014). The plutons constituting the Cerro Áspero batholith display polygonal contacts that are frequently discordant with respect to the mylonitic foliation of the GCSZ. These relationships, along with other field structures, evidence a fracture-controlled emplacement mechanism (stoping) at shallow crustal levels indicating late to post-kinematic origin with respect to that deformation (Pinotti et al., 2002, 2016), *i.e.*, the GCSZ was not operating, or at least waning, during the Cerro Áspero batholith emplacement. The field relationships, structural and microstructural evidence described above for leucogranites indicate that they were emplaced synkinematically with the ductile deformation of the GCSZ, during the onset of its development. This suggests that both magmatic rocks (leucogranites from the CPF and monzogranites from the Cerro Áspero batholith) are completely diachronic. Therefore, a crystallization age at ~370 Ma for leucogranites has no geological significance since the whole area was subjected to high structural levels (around 200 MPa) and the GCSZ activity had finished before the late Devonian (Steenken et al.,

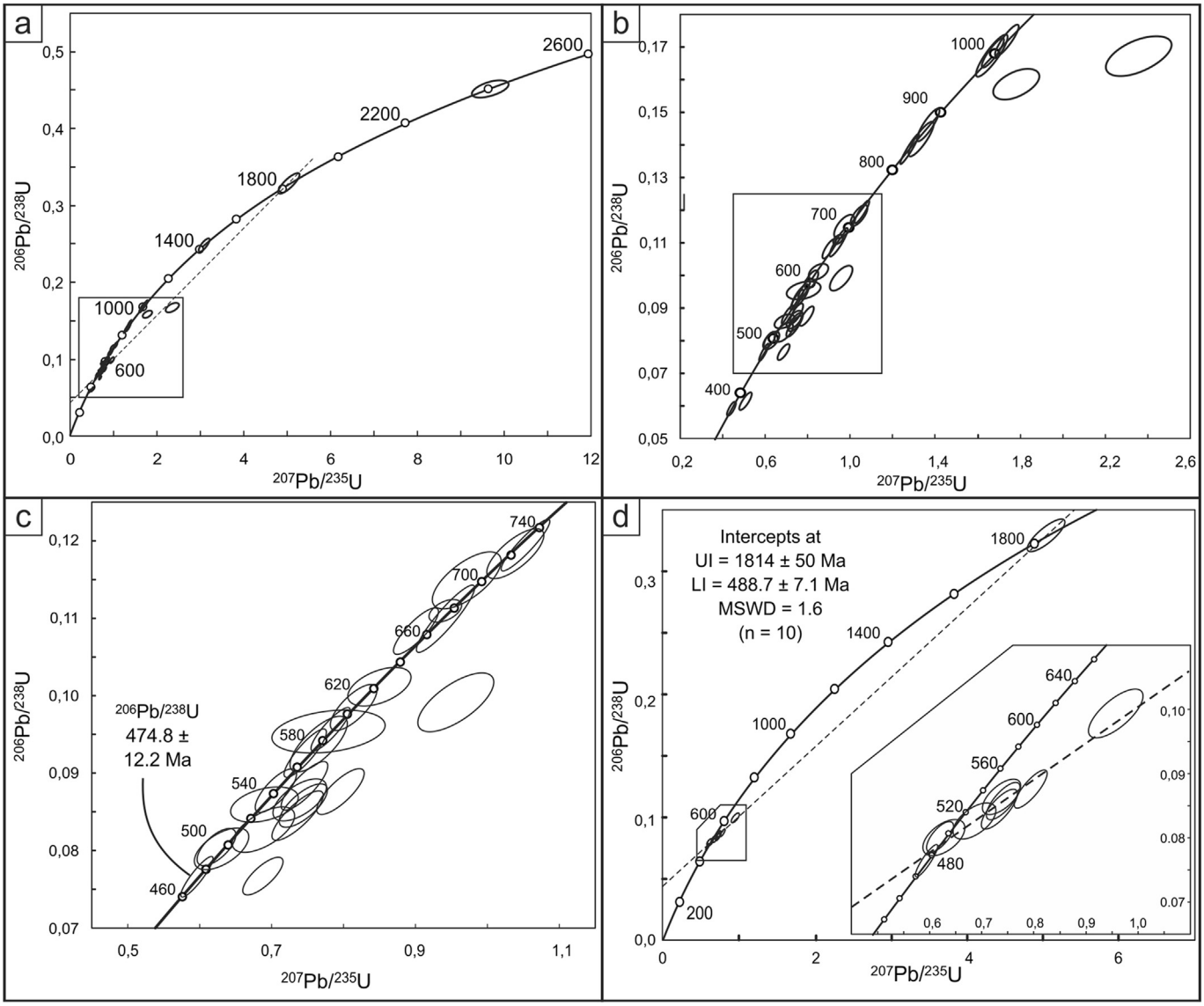

Fig. 6. Conventional concordia diagrams for leucogranites (sample 576), showing **a)** the whole data set obtained in the sample (rectangle shows the location of Fig. 6b); **b)** detail of the age range between ~370 and ~1000 Ma (rectangle shows the location of Fig. 6e); **c)** detail of the age range between ~450 and ~750 Ma, highlighting the crystallization age ($^{206}Pb/^{238}U$ age 474.8 ± 12.2 Ma). Error ellipses are plotted at 2σ. **d)** discordia line defined by clusters of non-concordant ages.

2010). Instead, it can be interpreted as a zircon crystal that experienced a reset in the U-Pb system during the Devonian magmatic event that led to the emplacement and crystallization of the Cerro Áspero batholith. This interpretation is supported by the morphological features of the zircon crystal from which they were obtained and the above mentioned geological arguments.

Discarding the above discussed Devonian ages, the youngest $^{206}Pb/^{238}U$ age is 474.8 ± 12.2 Ma (analysis 8-1; Table 2), which is considered the best constraint for the timing of the emplacement and crystallization of the leucogranites. The prismatic shape, broad parallel zoning and the complete lack of inclusions in the analyzed crystal suggest that no later modifications have occurred, and that a single event of crystallization was the responsible for its formation, arguing for a completely magmatic origin of this grain.

A regression line was calculated using a cluster of six discordia ages along with some other concordia analyses (Fig. 6d), obtaining an upper intercept of the concordia curve at 1814 ± 50 Ma and a lower intercept at 488.7 ± 7.1Ma (MSWD = 1.6). The lower interception ages correlates well, within uncertainties, to the 474.8 ± 12.2 Ma $^{206}Pb/^{238}U$ age of crystallization of the leucogranites.

The crystallization ages obtained for the granitic pegmatites and leucogranites are equivalent to each other. Furthermore, a strong genetic link between these rocks is also evidenced by field relationships, structural, microstructural and deformation history (Demartis et al., 2011; this work). All this information indicates that both rock types originated coevally, at around 474 Ma. This age perfectly correlates with the timing of the development of the Famatinian magmatic arc in different parts of Sierras Pampeanas and Famatina (Pankhurst et al., 1998, 2000; Sims et al., 1998; Baldo et al., 2003; Fanning et al., 2004; Steenken et al., 2006; Dahlquist et al., 2008; Ducea et al., 2010; Sfragulla, 2013; Morosini et al., 2017, Table 1). Linares and Latorre (1969) obtained an age of 480 ± 15 Ma from the Ángel pegmatite, central-southern CPF, by

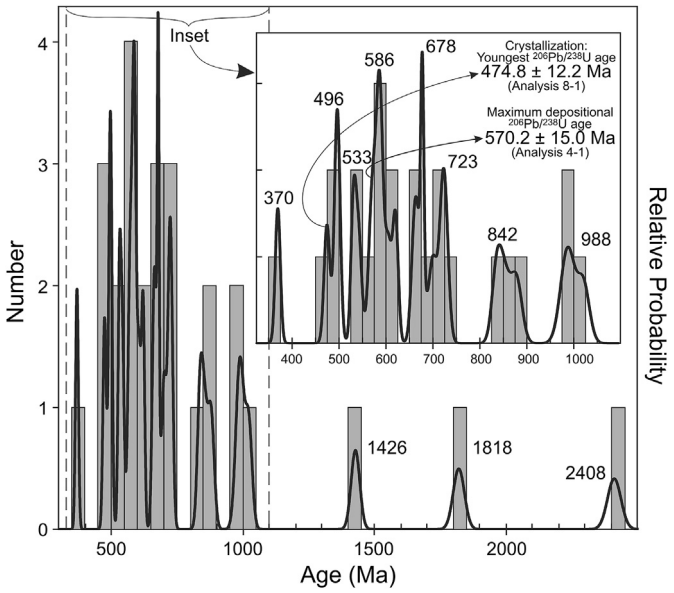

Fig. 7. Histogram (bin width of 50 Ma) combined with probability plot showing the distribution of the whole concordant zircon ages (degree of concordance between 90 and 110%) obtained for the leucogranite (sample 576). The inset amplifies the age range between 325 and 1100 Ma (bin width of 25 Ma) and remarks the crystallization and maximum depositional ages discussed in the text. Ages younger than 1000 Ma are $^{206}Pb/^{238}U$ data and ages older than 1000 Ma are $^{207}Pb/^{206}Pb$ data.

the Pb/U in uraninite method. Another two pegmatites from the northern CPF (Quebrada del Tigre and Cerro Blanco pegmatites) were analyzed by the same method, yielding 472 ± 25 and 477 ± 25 Ma, respectively. The ages obtained by Linares and Latorre (1969) are equivalent, within errors, with the 474 Ma age of crystallization obtained in this work.

5.2. Time constraints and exhumation rate for the GCSZ deformation

The age of ~474 Ma obtained for the crystallization of pegmatites and leucogranites is here considered a reasonable time constraint for the M3a-D3a ductile deformation of the GCSZ, since they were emplaced synkinematically with that event.

Two K/Ar muscovite-booklet ages of around 487 Ma from pegmatites located at the footwall of the GCSZ were obtained by Steenken et al. (2010), who interpreted these results as nearly crystallization ages since no deformation over 550 °C has affected the dated pegmatites. The pegmatites and leucogranites dated in our work crop out in the hanging wall of this shear zone and are strongly deformed from submagmatic to low temperature subsolidus conditions (Demartis et al., 2011; this work). Silurian ages (~435 Ma) obtained from igneous and metamorphic rocks also allowed Steenken et al. (2010) to propose a further reactivation of the GCSZ deformation during this time. Therefore, the whole dataset indicate that pegmatites from the footwall of the GCSZ (Steenken et al., 2010) were emplaced shortly before (~10 Ma earlier) than pegmatites and leucogranites from the hanging wall (this work). The synkinematic emplacement of these pegmatites and leucogranites, along with geochronological data presented here, suggest that the M3a-D3a ductile deformation of the GCSZ, coincident with the first phase of compression following Steenken et al. (2010), should have started between 487 and 474 Ma. Further reactivation of the shear zone during Silurian times (second phase of compression according to Steenken et al., 2010), affected the pegmatites and granites from both footwall and hanging wall, when the whole area cooled below the muscovite closing temperature. This second compression event may be correlated with the M3b-D3b retrograde deformation.

During the Famatinian orogeny, the GCSZ exhumed most of the crustal rocks that comprise the Sierra de Comechingones. Taking the crystallization ages and pressure conditions during the emplacement of both granitic pegmatites from the CPF and monzogranites from the Cerro Áspero batholith, an exhumation rate of the GCSZ can be calculated. The area comprising the Comechingones pegmatitic field was subjected to pressure conditions of 500 MPa (Demartis et al., 2010) at ~475 Ma (this work) and then it exhumed to a pressure around 200 MPa at ~370 Ma (Pinotti et al., 2006). Therefore, an approximate linear exhumation rate of 2.9 MPa/Ma can be established for the exhumation rate of this part of the Sierras Pampeanas between early Ordovician and late Devonian. Considering the average pressure gradient of 1GPa/35 km for the continental crust proposed by Dziewonski and Anderson (1981), this rate represents 0.10 mm/a. The calculated linear exhumation rate seems to be very low. However, the total amount of exhumation (~10.5 km) during this time span (from 475 to 370 Ma) was considerably high, and it probably occurred during successive short-lived phases of compression (Steenken et al., 2010) with much higher exhumation rates. The calculated value of total amount of exhumation (10.5 km) is consistent with the 9 km maximum vertical movement obtained by Whitmeyer and Simpson (2003) for the GCSZ in this region.

5.3. Inherited ages of the leucogranites

The origin of the large spread in inherited ages of the leucogranite sample (Figs. 6 and 7) is here explained by two sources: 1) detrital zircons constituting accessory mineral of the protolith, and 2) later metamorphic overgrowth.

The probability age distribution pattern for the leucogranites shows intense peaks at 496, 586 and 678 Ma, and subordinated peaks at 533, 723, 842, 988, 1426, 1818 and 2408 Ma (Fig. 7). This pattern strongly resembles those for metasedimentary rocks from the Pampean belt in the eastern Sierras Pampeanas (Fig. 8). Peaks around 580, 670 and 1000 Ma can be correlated with those of detrital zircon ages from metamorphic rocks in the northern part of the Sierras de Córdoba (Sims et al., 1998; Schwartz and Gromet, 2004; Iannizzotto et al., 2013; Escayola et al., 2007) and from the Ancasti formation, Catamarca province (Rapela et al., 2007, Fig. 8). Drobe et al. (2011) also measured very similar detrital ages in an orthogneiss of the Monte Guazú complex, in the southernmost part of the Sierras de Córdoba. The peak at ~1400 Ma was also obtained by Sims et al. (1998) in metasedimentary rocks of the Quilpo formation in the northern Sierras de Córdoba. Meanwhile, older inherited ages (peaks at ~1800 and ~2400 Ma) can be explained by sources with Paleoproterozoic and Mesoproterozoic ages, less statistically represented, but also obtained by other authors (Drobe et al., 2011). Steenken et al. (2006) also obtained similar detrital zircon ages from metasediments of the Conlara metamorphic complex, located a few kilometers to the west of the CPF, for which these authors suggest the connection with the Puncoviscana Formation.

The dominant peak of 533 Ma for inherited ages in the leucogranite sample (Fig. 7) also correlates with the timing of the metamorphic peak constrained for the Pampean regional metamorphism in several parts of the Sierras de Córdoba (Table 1).

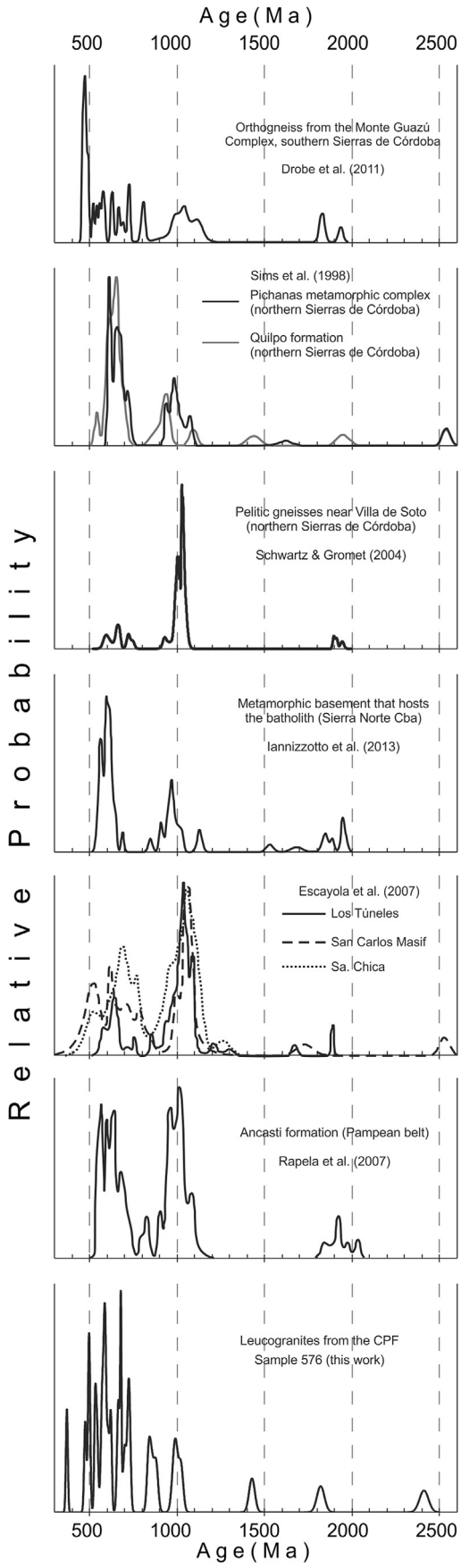

Texturally, the concordant inherited ages that range between 531 and 542 Ma (analyses 15-2 and 28-2 from sample 576, Table 2; Fig. 5) were obtained from spot analyses carried out in overgrowth rims that are interpreted as metamorphic overgrowths. Although Th abundances have not been measured, these rims mostly show dark grey colors in CL images indicating relatively low Th/U ratios, probably compatible with metamorphic growth.

Considering the previous evaluations, the range of inherited ages between 531 and 542 Ma represents the metamorphic overgrowth occurred during the Pampean orogeny, while the rest of the older ages (from 570 to 2408 Ma) corresponds to original detrital zircons of the protolith. Therefore, the youngest age for detrital zircons in the leucogranite sample ($^{207}Pb/^{206}Pb$ age of 549.1 ± 35.0 Ma; Table 2 and Fig. 7) would represent the maximum depositional age for the sediments that were metamorphosed during Pampean orogeny. This depositional age overlaps, within errors, with that estimated by Schwartz and Gromet (2004) for metasedimentary rocks of the Pampean belt in northern Sierras de Córdoba.

The strong similarities in the distribution of detrital zircon ages, maximum depositional age and timing of the metamorphic overgrowths suggest that the protoliths that melted to form the leucogranites and pegmatites of the CPF during the Famatinian orogeny would have been (at least partly) equivalents to the gneisses, migmatites and schists that crop out in many parts of the Pampean belt (Sierras de Córdoba and Catamarca).

6. Concluding remarks

(1) The investigated granitic pegmatites and leucogranites from the CPF crystallized at 474 Ma. The field relationships, structural and petrographic evidence, and the obtained geochronological data allowed us to establish that the granitic pegmatites and leucogranites from the CPF formed coevally in the inner Famatinian magmatic arc.

(2) Since pegmatites and leucogranites from the CPF were synkinematically emplaced with the main ductile M3a-D3a deformational event of the GCSZ, the previous ages also constitute a reasonable timing for this event. The age and pressure conditions of both the GCSZ and Cerro Áspero batholith were used to calculate a linear exhumation rate of around 0.10 mm/a and a total amount of exhumation of 10.5 km for this part of the Sierras Pampeanas between early Ordovician and late Devonian. The amount of granitic and pegmatitic rocks involved in this magmatic event suggests a strong linkage with the development of the crustal-scale GCSZ, which favored in a feedback relationship the ascent and emplacement of granitic melts (Demartis et al., 2011).

(3) The strong inheritance of zircon ages and the distribution pattern obtained in leucogranites suggest the involvement of protoliths that could probably be equivalent to the currently outcropping Pampean metamorphic basement.

Fig. 8. Comparison between probability plots of the leucogranite from the CPF obtained in this work (Fig. 7) and those obtained by other authors for detrital zircon ages in different metasedimentary rocks of the Pampean metamorphic belt in Córdoba and Catamarca provinces, summarized in Table 1. Data are compiled from: Rapela et al. (2007) for the Ancasti formation (Catamarca); Escayola et al. (2007) for the Sierra Chica, San Carlos massif and Los Túneles (Sierras de Córdoba); Iannizzotto et al. (2013) for the host metamorphic rocks of the Sierra Norte batholith (Córdoba); Schwartz and Gromet (2004) for pelitic gneisses near the Villa de Soto village (Córdoba) (probability density diagram plotted using data from Table 1 of the mentioned authors); Sims et al. (1998) for the Pichanas metamorphic complex and Quilpo formation (Córdoba); Drobe et al. (2011) for an orthogneiss from the Monte Guazú complex (Córdoba).

Acknowledgments

The authors want to thank the two reviewers and the Regional Editor, Victor Ramos, for their comprehensive and certain suggestions, which have greatly helped to improve the manuscript. This work was financially supported by the following institutions: SECYT-UNRC (project PPI 18/C456), CONICET (project PIP 088), and FONCYT-ANPCyT (project PICT 0910/13).

References

Angelelli, V., 1950. Recursos minerales de la República Argentina – I – Yacimientos Metalíferos. Museo Argentino de Ciencias Naturales 'Bernardino Rivadavia', Revista Ciencias Geológicas, vol. 2, 543 pp. Buenos Aires.

Baldo, E.G., Fanning, C.M., Rapela, C.W., Pankhurst, R.J., Casquet, C., Galindo, C, C., 2003. U-Pb Shrimp dating of rhyolite volcanism in the Famatinian belt and K-bentonites in the Precordillera. In: Albanesi, G.L., Beresi, M.S., Peralta, S.H. (Eds.), Ordovician From the Andes. Serie de Correlación Geológica (INSUGEO-UNTucumán), vol. 17, pp. 41–46.

Bouchez, J.L., Delas, C., Gleizes, G., Nedelec, A., Cuney, M., 1992. Submagmatic microfractures in granites. Geology 20, 35–38. http://dx.doi.org/10.1130/0091-7613(1992)020<0035:smig>2.3.co;2.

Černý, P., y Ercit, T.S., 2005. The classification of granitic pegmatites revisited. Can. Mineral. 43, 2005–2026. http://dx.doi.org/10.2113/gscanmin.43.6.2005.

Cristofolini, E.A., Fagiano, M., Pinotti, L.P., 2008. Fábricas migmáticas y miloníticas: un análisis comparativo, norte de Sierra de Comechingones, Córdoba. In: XVII Congreso Geológico Argentino, 1334. San Salvador de Jujuy, Argentina.

Cristofolini, E.A., Otamendi, J.E., Walker Jr., B.A., Tibaldi, A.M., Armas, P., Bergantz, G.W., Martino, R.D., 2014. A Middle Paleozoic shear zone in the Sierra de Valle Fértil, Argentina: records of a continent-arc collision in the Famatinian margin of Gondwana. J. S. Am. Earth Sci. 56, 170–185. http://dx.doi.org/10.1016/j.jsames.2014.09.010.

Dahlquist, J.A., Pankhurst, R.J., Rapela, C.W., Galindo, C., Alasino, P., Fanning, C.M., Saavedra, J., Baldo, E., 2008. New SHRIMP U-Pb data from the Famatina complex: constraining early–Mid Ordovician Famatinian magmatism in the Sierras Pampeanas, Argentina. Geol. Acta 6 (4), 319–333.

Demartis, M., 2010. Emplazamiento y petrogénesis de las pegmatitas y granitoides asociados. PhD Thesis. Library of the Universidad Nacional de Río Cuarto, Sector central de la Sierra de Comechingones, Córdoba, Argentina (unpublished). 265 pp.

Demartis, M., Coniglio, J.E., Pinotti, L.P., D'Eramo, F.J., Agulleiro Insúa, L.A., Muñoz, A.A., Petrelli, H.A., 2010. Modelado de fluidos de las pegmatitas de la porción sur del distrito Comechingones, Córdoba, a partir de nuevos datos de isótopos estables. In: X Congreso de Mineralogía y Metalogenia, Río Cuarto. Actas, pp. 171–178.

Demartis, M., Pinotti, L.P., Coniglio, J.E., D'Eramo, F.J., Tubía, J.M., Aragón, E., Agulleiro Insúa, L.A., 2011. Ascent and emplacement of pegmatitic melts in a major reverse shear zone (Sierras de Córdoba, Argentina). J. Struct. Geol. 33 (9), 1334–1346. http://dx.doi.org/10.1016/j.jsg.2011.06.008.

Demartis, M., Melgarejo, J.C., Colombo, F., Alfonso, P., Coniglio, J.E., Pinotti, L.P., D'Eramo, F.J., 2014. Extreme F activities in late pegmatitic events as a key factor for LILE and HFSE enrichment: the Ángel pegmatite, Central Argentina. Can. Mineral. 52 (2), 247–269. http://dx.doi.org/10.3749/canmin.52.2.247.

D'Eramo, F.J., Tubía, J.M., Pinotti, L.P., Vegas, N., Coniglio, J., Demartis, M., Aranguren, A., Basei, M., 2013. Granite emplacement by crustal boudinage: example of the Calmayo and El Hongo plutons (Córdoba, Argentina). Terra Nova 25 (5), 423–430. http://dx.doi.org/10.1111/ter.12053.

D'Eramo, F.J., Pinotti, L.P., Bonalumi, A., Sfragulla, J., Demartis, M., Coniglio, J.E., Baldo, E.G., 2014. El magmatismo ordovícico en las Sierras Pampeanas de Córdoba. In: Martino, R.D., Guereschi, A.B. (Eds.), Relatorio del XIX Congreso Geológico Argentino: Geología y Recursos Naturales de la provincia de Córdoba. Asociación Geológica Argentina, Part I, pp. 233–254.

Drobe, M., López de Luchi, M., Steenken, A., Wemmer, K., Naumann, R., Frei, R., Siegesmund, S., 2011. Geodynamic evolution of the eastern Sierras Pampeanas (central Argentina) based on geochemical, Sm–Nd, Pb–Pb and SHRIMP data. Int. J. Earth Sci. Geol. Rundschau) 100, 631–657. http://dx.doi.org/10.1007/s00531-010-0593-3.

Ducea, M.N., Otamendi, J.E., Bergantz, G., Stair, K., Valencia, V., Gehrels, G., 2010. Timing constraints on building an intermediate plutonic arc crustal section: U-Pb zircon geochronology of the Sierra Valle Fértil, Famatinian Arc, Argentina. Tectonics 29, TC4002. http://dx.doi.org/10.1029/2009TC002615.

Dziewonski, A.M., Anderson, D.L., 1981. Preliminary reference Earth model. Phys. Earth Planet. Interiors 25 (4), 297–356. http://dx.doi.org/10.1016/0031-9201(81)90046-7.

Escayola, M.P., Pimentel, M.M., Armstrong, R., 2007. Neoproterozoic backarc basin: sensitive high-resolution ion microprobe U-Pb and Sm-Nd isotopic evidence from the Eastern Pampean Ranges, Argentina. Geology 35, 495–498. http://dx.doi.org/10.1130/G23549A.1.

Fagiano, M., 2007. Geología y Petrología del basamento cristalino de las Albahacas, sur de la Sierra de Comechingones, Córdoba. Tesis Doctoral (inédito). Dpto. de Geología, FCEFQyN, Universidad Nacional de Río Cuarto (Biblioteca), 380pp.

Fagiano, M., Martino, R., 2004. Cinemática y petrología de la faja de cizalla Guacha Corral en el extremo austral de la sierra de Comechingones, Provincia de Córdoba, vol. 7. Revista de la Asociación Geológica Argentina, Serie D, Special Publication, pp. 45–50.

Fagiano, M., Pinotti, L.P., Esparza, A.M., 2004. Metamorfismo, deformación y magmatismo asociados en el tramo medio de la Sierra de Comechingones, provincia de Córdoba. In: VII Congreso de Mineralogía y Metalogenia, pp. 315–320 (Río Cuarto, Argentina).

Fanning, C.M., Pankhurst, R.J., Rapela, C.W., Baldo, E.G., Casquet, C., Galindo, C., 2004. K-bentonites in the Argentine Precordillera contemporaneous with rhyolite volcanism in the Famatinian arc. J. Geol. Soc. Lond. 161, 747–756. http://dx.doi.org/10.1144/0016-764903-130.

Galliski, M., 1994. La Provincia Pegmatítica Pampeana. I: tipología y distribución de sus distritos económicos. Rev. la Asoc. Geol. Argent. 49 (1–2), 99–112.

Hub, C.C., 1994. Estudio geológico-económico de pegmatitas del Distrito Comechingones. Unpublished report. CONICOR, p. 156. Córdoba.

Hub, C.C., 1995. Estudio geológico-económico de pegmatitas del Distrito Comechingones. Unpublished report. CONICOR, p. 172. Córdoba.

Iannizzotto, N.F., Rapela, C.W., Baldo, E.G., Galindo, C., Fanning, C.M., 2013. The Sierra Norte–Ambargasta Batholith: Cambrian magmatism formed in a transpressional belt along the western edge of the Río de la Plata cratón? J. S. Am. Earth Sci. 42, 127–142. http://dx.doi.org/10.1016/j.jsames.2012.07.009.

Ježek, P., Willner, A.P., Aceñolaza, F.G., Miller, H., 1985. The Puncoviscana trough - a large basin of late precambrian to early cambrian age on the pacific edge of the Brazilian shield. Geol. Rundsch. 74 (3), 573–584. http://dx.doi.org/10.1007/BF01821213.

Kooijman, E., Berndt, J., Mezger, K., 2012. U-Pb dating of zircon by laser ablation ICP-MS: recent improvements and new insights. Eur. J. Mineral. 24, 5–21. http://dx.doi.org/10.1127/0935-1221/2012/0024-2170.

Linares, E., Latorre, C.O., 1969. Edades potasio-argón y plomo-alfa de rocas graníticas de las provincias de Córdoba y San Luis. In: IV Jornadas Geológicas Argentinas, II, pp. 195–204 (Mendoza, Argentina).

Lira, R., Sfragulla, J., 2014. El magmatismo Devónico-Carbonífero: el batolito de Achala y plutones menores al norte del cerro Champaquí. In: Martino, R.D., Guereschi, A.B. (Eds.), Relatorio del XIX Congreso Geológico Argentino: Geología y Recursos Naturales de la provincia de Córdoba. Asociación Geológica Argentina, Part I, pp. 293–347.

Martino, R., 2003. Las fajas de deformación dúctil de las Sierras Pampeanas de Córdoba: una reseña general. Rev. la Asoc. Geol. Argent. 58 (4), 549–571.

Martino, R.D., Kraemer, P., Escayola, M., Giambastiani, M., Arnosio, M., 1995. Transecta de las Sierras Pampeanas de Córdoba a los 32°00' LS. Rev. la Asoc. Geol. Argent. 50, 60–77.

Methol, E.J., 1971. Descripción Geológica de la Hoja 22h, Santa Rosa, Provincias de Córdoba y San Luis. In: Carta Geológico-Económica de la República Argentina - Escala 1:200.000. Dirección Nacional de Geología y Minería, Boletín N°, vol. 124, p. 73 (Buenos. Aires).

Miller, J.S., Matzel, J.E.P., Miller, C.F., Burgess, S.D., Miller, R.B., 2007. Zircon growth and recycling during the assembly of large, composite arc plutons. J. Volcanol. Geotherm. Res. 167, 282–299. http://dx.doi.org/10.1016/j.jvolgeores.2007.04.019.

Morosini, A., Ortiz Suárez, A., 2010. La deformación famatiniana del Granito La Escalerilla, sierra de San Luis. Rev. la Asoc. Geol. Argent. 67 (4), 481–493.

Morosini, A., Ortiz Suárez, A., Otamendi, J.E., Pagano, D.S., Ramos, G., 2017. La Escalerilla pluton, San Luis Argentina: the orogenic and post-orogenic magmatic evolution of the famatininan cycle at Sierras de San Luis. J. S. Am. Earth Sci. http://dx.doi.org/10.1016/j.jsames.2016.12.001.

Morteani, G., Eichinger, F., Götze, J., Tarantola, A., Müller, A., 2012. Evaluation of the Potential of the Pegmatitic Quartz Veins of the Sierra de Comechigones (Argentina) as a Source of High Purity Quartz by a Combination of LA-ICP-MS, ICP, Cathodoluminescence, Gas Chromatography, Fluid Inclusion Analysis, Raman and FTIR spectroscopy. In: Götze, J., Möckel, R. (Eds.), Quartz: Deposits, Mineralogy and Analytics. Springer Geology. Springer, Berlin, Heidelberg, pp. 119–137. http://dx.doi.org/10.1007/978-3-642-22161-3_5.

Morteani, G., Eichinger, F., Tarantola, A., Müller, A., Götze, J., Sfragulla, J.A., 2016. The synorogenic pegmatitic quartz veins of the Guacha Corral Shear zone (Sierra de Comechingones, Argentina): a textural, chemical, isotopic, cathodoluminescence and fluid inclusion study. Chem. Der Erde - Geochem. 76 (3), 391–404. http://dx.doi.org/10.1016/j.chemer.2015.09.001.

Otamendi, J.E., Castelarini, P.A., Fagiano, M., Demichelis, A., y Tibaldi, A., 2004. Cambrian to Devonian geologic evolution of the Sierra de Comechingones, eastern Sierras Pampeanas: evidence for the development and exhumation of continental crust on the proto-pacific margin of Gondwana. Gondwana Res. 7 (4), 1143–1155. http://dx.doi.org/10.1016/S1342-937X(05)71090-X.

Otamendi, J.E., Vujovich, G.I., de la Rosa, J.D., Tibaldi, A.M., Castro, A., Martino, R.D., Pinotti, L.P., 2009. Geology and petrology of a deep crustal zone from the Famatinian paleo-arc, Sierras Valle Fértil-La Huerta, San Juan, Argentina. J. S. Am. Earth Sci. 27 (4), 258–279. http://dx.doi.org/10.1016/j.jsames.2008.11.007.

Pankhurst, R.J., Rapela, C.W., Saavedra, J., Baldo, E., Dahlquist, J., Pascua, I., Fanning, C.M., 1998. The Famatinian magmatic arc in the central Sierras Pampeanas: an Early to Mid-Ordovician continental arc on the Gondwana margin. In: Pankhurst, R.J., y Rapela, C.W. (Eds.), The Proto-Andean Margin of Gondwana. Geological Society, vol. 142. Special Publication, London, pp. 343–367. http://dx.doi.org/10.1144/GSL.SP.1998.142.01.17.

Pankhurst, R.J., Rapela, C.W., Fanning, C.M., 2000. Age and origin of coeval TTG, I- and S-type granites in the Famatinian belt of NW Argentina. Trans. R. Soc. Edinb.

Earth Sci. 91, 151–168. http://dx.doi.org/10.1130/0-8137-2350-7.151.
Pinotti, L.P., D'Eramo, F.J., Weinberg, R.F., Demartis, M., Tubía, J.M., Coniglio, J.E., Radice, S., Maffini, M.N., Aragón, E., 2016. Contrasting magmatic structures between small plutons and batholiths emplaced at shallow crustal level (Sierras de Córdoba, Argentina). J. Struct. Geol. 92, 46–58. http://dx.doi.org/10.1016/j.jsg.2016.09.009.
Pinotti, L.P., Tubía, J.M., D'Eramo, F.J., Vegas, N., Sato, A.M., Coniglio, J.E., y Aranguren, A., 2006. Structural interplay between plutons during the construction of a batholith (Cerro Aspero batholith, Sierras de Córdoba, Argentina). J. Struct. Geol. 28 (5), 834–849. http://dx.doi.org/10.1016/j.jsg.2006.02.004.
Pinotti, L.P., Coniglio, J.E., D'Eramo, F.J., Demartis, M., Otamendi, J.E., Fagiano, M.R., Zambroni, N.E., 2014. El magmatismo devónico: geología del batolito de Cerro Áspero. In: Martino, R.D., Guereschi, A.B. (Eds.), Relatorio del XIX Congreso Geológico Argentino: Geología y Recursos Naturales de la provincia de Córdoba. Asociación Geológica Argentina, Part I, pp. 255–276.
Pinotti, L.P., Coniglio, J.E., Esparza, A.M., D'Eramo, F.J., y Llambías, E.J., 2002. Nearly circular plutons emplaced by stoping at shallow crustal levels, Cerro Aspero batholith, Sierras Pampeanas de Córdoba, Argentina. J. S. Am. Earth Sci. 15, 251–265. http://dx.doi.org/10.1016/S0895-9811(02)00033-0.
Radice, S., 2015. Estudio petro-estructural de la Faja de Cizalla Guacha Corral y su relación con variaciones químicas, magnéticas y gravimétricas, Sierra de Comechingones, Córdoba, Argentina. PhD Thesis. Library of the Universidad Nacional de Río Cuarto (unpublished). 324 pp.
Radice, S., Arangue, J., Fagiano, M., Pinotti, L., Cristofolini, E., 2012. Análisis petrológico estructural del basamento encajonante del Batolito Cerro Áspero, Sierra de Comechingones, Córdoba. Ser. Correlación Geol. 28, 09–22.
Radice, S., Arangue, J., Fagiano, M., Pinotti, L.P., Cristofolini, E., 2015. Microfábricas de deformación del basamento metamórfico, sector centro-oriental de la Sierra de Comechingones, Córdoba. Rev. la Asoc. Geol. Argent. 72 (2), 157–166.
Ramos, V.A., 1999. Rasgos estructurales del territorio argentino. 1) Evolución tectónica de la Argentina. Geología Argentina. SEGEMAR - Instituto de Geología y Recursos Minerales, Buenos Aires. Anales 29 (24), 715–759.
Rapela, C.W., Pankhurst, R.J., Casquet, C., Baldo, E., Saavedra, J., Galindo, C., y Fanning, C.M., 1998. The Pampean orogeny of the southern proto-Andes: Cambrian continental collision in the Sierras de Córdoba. In: Pankhurst, R.J., y Rapela, C.W. (Eds.), The Proto-Andean Margin of Gondwana. Geological Society, vol. 142. Special Publication, London, pp. 181–217. http://dx.doi.org/10.1144/GSL.SP.1998.142.01.10.
Rapela, C.W., Pankhurst, R.J., Casquet, C., Fanning, C.M., Baldo, E.G., González-Casado, J.M., Galindo, C., Dahlquist, J., 2007. The Río de la Plata craton and the assembly of SW Gondwana. Earth Sci. Rev. 83 (1–2), 49–82. http://dx.doi.org/10.1016/j.earscirev.2007.03.004.
Rinaldi, C.A., 1968. Estudio de las pegmatitas uraníferas de las Sierras de Comechingones, provincia de Córdoba. Rev. Asoc. Geol. Argent. 23 (3), 161–195.
Rinaldi, C.A., 1969. Estudio de las pegmatitas uraníferas de las sierras Comechingones, Provincia de Córdoba. Comisión Nacional de Energía Atómica, Buenos Aires, p. 56. Unpublished report N° 256.
Sato, A.M., González, P.D., Llambías, E.J., 2003. Evolución del orógeno Famatiniano en la Sierra de San Luis: magmatismo de arco, deformación y metamorfismo de bajo a alto grado. Rev. Asoc. Geol. Argent. 58, 487–504.
Schwartz, J.J., Gromet, L.P., 2004. Provenance of Late Proterozoic-early Cambrian basin, Sierras de Córdoba, Argentina. Precambrian Res. 129, 1–21. http://dx.doi.org/10.1016/j.precamres.2003.08.011.
Sfragulla, J.A., 2013. Plutonismo de las Sierras de Altautina y Quebrada del Tigre, Sierras Pampeanas Orientales. PhD Thesis. Universidad Nacional de Salta, Argentina (unpublished). 308 pp.
Siegesmund, S., Steenken, A., Martino, R., Wemmer, K., López de Luchi, M.G., Frei, R., Presnyakow, S., Guereschi, A., 2010. Time constraints on the tectonic Evolution of the Eastern Sierras Pampeanas (Central Argentina). Int. J. Earth Sci. 99 (6), 1199–1226. http://dx.doi.org/10.1007/s00531-009-0471-z.
Simpson, C., Law, R.D., Gromet, L.P., Miró, R., Nothrup, C.J., 2003. Paleozoic deformation in the Sierras de Córdoba and Sierra de las Minas, eastern Sierras Pampeanas, Argentina. – J. S. Am. Earth Sci. 15, 749–764.
Sims, J., Ireland, T.R., Camacho, A., Lyons, P., Pieters, P.E., Skirrow, R., Stuart-Smith, P.G., Miró, R., 1998. U–Pb, Th–Pb, and Ar–Ar geochronology from the Southern Sierras Pampeanas, Argentina: implications for the Paleozoic tectonic evolution of the western Gondwana margin. In: Pankhurst, R.J., y Rapela, C.W. (Eds.), The Proto-Andean Margin of Gondwana. Geological Society, vol. 142. Special Publication, London, pp. 259–281. http://dx.doi.org/10.1144/GSL.SP.1998.142.01.13.
Steenken, A., Siegesmund, S., López de Luchi, M.G., Frei, R., Wemmer, K., 2006. Neoproterozoic to early Palaeozoic events in the Sierra de San Luis: implications for the Famatinian geodynamics in the Eastern Sierras Pampeanas (Argentina). J. Geol. Soc. 163, 965–982. http://dx.doi.org/10.1144/0016-76492005-064.
Steenken, A., Wemmer, K., Martino, R.D., López de Luchi, M.G., Guereschi, A., Siegesmund, S., 2010. Post-pampean cooling and the uplift of the Sierras Pampeanas in the west of Córdoba (central Argentina). Neues Jahrb. für Geol. Paläontologie – Abh. 256 (2), 235–255. http://dx.doi.org/10.1127/0077-7749/2010/0094.
Stuart-Smith, P.G., Camacho, A., Sims, J.P., Skirrow, R.G., Lyons, P., Pieters, P.E., Black, L., Miró, R., 1999. Uranium-lead dating of felsic magmatic cycles in the southern Sierras Pampeanas, Argentina: implications for the tectonic development of the proto- Andean Gondwana margin. In: Ramos, V.A., Keppie, J.D. (Eds.), Laurentia-Gondwana before Pangea. Geological Society of America Special Paper, vol. 336, pp. 87–114.
Toselli, A.J., 1990. Metamorfismo del Ciclo Pampeano. In: Acenolaza, F.G., Miller, H., Toselli, A.J. (Eds.), El Ciclo Pampeano en el Noroeste Argentino. Universidad Nacional de Tucumán, Serie Correlación Geológica, vol. 4, pp. 181–198.
Whitmeyer, S.J., Simpson, C., 2003. High strain-rate deformation fabrics characterize a kilometers-thick Paleozoic fault zone in the Eastern Sierras Pampeanas, central Argentina. J. Struct. Geol. 25, 909–922. http://dx.doi.org/10.1016/S0191-8141(02)00118-9.